Last Millennium Drought-inducing Teleconnections of the West Pacific Gradient during ENSO

Jens Zinke (jz262@leicester.ac.uk)
University of Leicester
Stuart A. Browning
Risk Frontiers
Andrew Hoell
NOAA, Physical Sciences Laboratory
Ian D. Goodwin
UNSW Sydney

Research Article

Keywords: ENSO, Walker Circulation, Western Pacific, sea surface temperature, paleoclimate, proxies, drought, teleconnections

Posted Date: April 21st, 2021

DOI: https://doi.org/10.21203/rs.3.rs-440316/v1

Abstract

Conflicting evidence points to either a strengthening or weakening Walker Circulation over the 20th century based on changes in sea surface temperature and sea level pressure gradients between the western and eastern Pacific. Since small changes in Pacific temperature gradients connected with the El Niño Southern Oscillation (ENSO) are related to global climate anomalies, it is of paramount importance to develop robust indices of their past behaviour. Here, we reconstruct the difference in sea surface temperature between the west and central Pacific during ENSO based on the Last Millennium Paleo Hydrodynamics Data Assimilation since 1000 AD. We demonstrate that the strength of the West Pacific Gradient (WPG) is related to stronger atmospheric circulation and remote precipitation anomalies during both historical El Niño and La Niña events and societally relevant drought teleconnections. A strong negative WPG coupled with a strong zonal Pacific temperature gradient is associated with enhanced megadroughts between 1400 AD and the late 16th century. The 20th century stands out as the period with most extreme swings between positive and negative WPG conditions. We conclude that the WPG serves as a powerful index of Pacific Walker Circulation variability and their associated global climate teleconnections.

Introduction

A lack of long instrumental climate records from the Indo-Pacific warm pool and the tropical Pacific, the heat engines of the global climate system and an essential player in global rainfall/drought cycles, is a main problem for reducing uncertainties in model-based climate change process studies and projections and to successfully plan for the future. The Maritime Continent (MC) plays a crucial part in the global hydrological variability through its influence on the Indo-Pacific Walker circulation (Neal & Slingo, 2003) collocating within the Indo-Pacific Warm Pool, where sea surface temperatures (SST) exceed 28°C associated with strong convective rainfall year-round. The Maritime Continent includes the archipelagos of Indonesia, Malaysia, New Guinea and the surrounding shallow seas. On its margins the MC is collocated within major centers of strong interannual SST variability in the Pacific. To the east, the western pole of the ENSO-SST anomalies (Niño4 and Niño3.4 regions; Kaplan et al., 1998) straddles the MC and have the strongest influence on MC precipitation between austral winter and spring. The convective activity over the Maritime Continent associated with ENSO is intimately linked to large- scale variations in the climate system and global rainfall-drought patterns in austral summer (Neal & Slingo, 2003). This includes the Asian Monsoon, African Monsoon, Austral-Asian Monsoon and the American Monsoon systems, all intimately linked via changes in the Walker Circulation (Krishnan et al., 2006; Tokinaga et al., 2012; Annamalei et al., 2013; Hoell and Funk, 2013; Ratna et al., 2016). However, correctly simulating precipitation across the MC in climate models and its impact on the Pacific Walker Circulation (PWC) presents a major challenge due to its topographic complexity often resulting in biased estimates of MC convective activity (Neal & Slingo, 2003; Qian, 2008). The same holds for air temperatures across the MC. Furthermore, conflicting evidence points to either a strengthening or weakening PWC over the 20th century based on changes in SST and SLP gradients between the western and eastern Pacific

(Karnauskas et al., 2009; Tokinaga et al., 2012; Coats & Karnauskas, 2017; L'Heureux et al., 2013; Seager et al., 2019; Chung et al., 2020). The difficulty to establish the correct sign of tropical Pacific SST gradient changes lies in the sparseness of data and differences between observational datasets which apply varying methods to correct observational biases, especially during the World War II period and pre-1880 (Coats & Karnauskas, 2017; Pfeiffer et al., 2017). The uncertainties in SST measurements also hamper our understanding of the link between changes in ENSO and tropical mean SST on decadal to centennial scales (Compo & Sardeshmukh, 2010; Solomon & Newman, 2012). Several ENSO reconstructions based on multi- or univariate proxy archives have provided invaluable insights into the past behaviour of the ENSO system and underlying centennial and decadal mean state changes (Stahle et al., 1998; Mann et al., 2000; McGregor et al., 2010; Wilson et al., 2010; Li et al., 2011, 2013; Emile-Geay et al., 2013a, b). However, ENSO reconstructions do not fully agree on El Niño or La Niña mean states and partly consider either the centre of action in the Niño3.4 domain, the distinction between EP and CP ENSO patterns and/or teleconnected regions.

Since small changes in Pacific SST gradients connected with ENSO are related to global climate anomalies, it is of paramount importance to develop robust indices of their past behaviour. New research has shown that the temperature difference between the westernmost Pacific and the central tropical Pacific region (hereafter West Pacific Gradient or WPG) plays a pivotal role in the global climate teleconnections (Hoell and Funk, 2013; Cai et al., 2015). The WPG was defined as the standardized difference between the central Pacific (Niño4 region; 5°S-5°N, 160–210°E) and western Pacific SST (0–10°N, 130–150°E) between 1854 and present from ERSSTv3b (Smith et al., 2008). Hoell and Funk (2013) and Hoell et al. (2014a, b) demonstrated that during both El Niño and La Niña events the global impacts in terms of atmospheric circulation and precipitation anomalies were larger when the SST anomalies in the west Pacific were strongly opposing those in the central Pacific than when the west Pacific SST anomalies were near neutral. These studies show that the SST gradient between the central (Niño4 region) and the western Pacific was an important measure of interannual to multi-decadal Pacific climate variability in addition to any previously derived metric of ENSO (Kaplan et al., 1998) or combination of ENSO metrics (see Table 2 of Hoell and Funk, 2013; Zinke et al., 2015). Furthermore, the spatial correlation patterns between the WPG with global air temperatures and SLP grid points resembles the pattern observed for using the zonal (West minus East) Pacific SST and SLP gradient used to define the PWC (Fig. 1).

Recent changes in the WPG due to strong WP warming and more frequent La Niña events after the Indo-Pacific decadal climate regime shift of the late 1990s to its La Nina-like phase (Feng et al., 2015; Lyon et al., 2014; Kataoka et al., 2014), are driving significant thermal anomalies impacting downstream coral reef ecosystems over several thousands of kilometres from the Indonesian seas to the southern coast of Western Australia and along the southwest Pacific. The abrupt rise in West Pacific SST in the late 1990s was also addressed by recent studies (Compo & Sardeshmukh, 2010; Solomon & Newman, 2012). Hoell and Funk (2013) showed that the abrupt warming of the West Pacific has resulted in a more negative WPG, which in turn has forced strong drought-inducing teleconnections across the Northern Hemisphere and the circum-Indian Ocean. Furthermore, Funk & Hoell (2015) showed evidence for a Western Pacific

warming mode with a V-shaped SST pattern radiating from the MC towards the extratropics which tracks with anthropogenic radiative forcing associated with drought-inducing atmospheric circulation changes. Recently, Cai et al. (2015) showed, for a subset of CMIP5 models, a high likelihood of a more intense WPG between the Maritime continent and the central Pacific and intensified La Niña events in 21st century projections with drought-inducing teleconnections, further highlighting the importance of the WPG in modulating PWC strength.

Consequently, this study aims to provide a reconstruction of the WPG and related tropical climate indices for the past Millennium to draw novel insights into past tropical climate variability. We make use of the Last Millennium reconstruction from PHYDA based on the PAGES2K data archive which contains a multivariate proxy data array to assess the interannual and decadal variability in the WPG, Maritime Continent (MC) temperatures, the Niño4 and Niño3.4 regions and the PWC at annual resolution since 1000 AD. We will demonstrate that the WPG is a powerful index which tracks past ENSO, tropical Pacific SST and SLP gradients, the PWC and their associated climate teleconnections. Our results reveal distinct periods of persistent El Niño or La Niña-like conditions during the past Millennium associated with shifts in the strength of the PWC and MC temperatures affecting global climate and drought ocurrences.

Results

Tropical Pacific SST is characterized by a zonal SST gradient (Fig. 1a) which strongly resembles the spatial SST pattern related to the WPG based on ERSST (Fig. 1b; Hoell & Funk, 2013). Results for the observed WPG based on definition by Cai et al. (2015) are similar, we therefore focus on the Hoell & Funk (2013) WPG (hereafter WPG_{obs}) for most of study. The typical horseshoe pattern in SST related to ENSO emerges in both spatial correlations. Our reconstructed PHYDA-derived WPG based on the definitions by Hoell & Funk (2013) (hereafter PWPG-HF; see **Fig. S1** for WPG Cai et al., 2015) revealed close agreement in reconstructed amplitude variations with the Niño3.4 index (Kaplan et al., 1998) based on observational data from 1854 onwards (Fig. 1c-e; **Fig. S1**). The PWPG-HF shows partially higher amplitude variations then the observational WPG. The PWPG-HF has higher variability then the Niño3.4 index (Fig. 1d) which also holds for the WPG_{obs} and PHYDA WPG Cai (hereafter PWPG-C; Fig. 1e; **Fig. S1**). We find a significant correlation between WPG_{obs} and Niño3.4 indices with our reconstructed WPG indices between 1850 and 2000 (**Fig. S2**). The PWPG-HF and PWPG-C show similarly strong correlations with the WPG_{obs} and Niño3.4 indices (**Figs. S3**). We also identified co-variability between the zonal Pacific SST (ZG_{sst}) and SLP (ZG_{slp}) gradients (definitions of L'Hereux et al., 2013; Coats & Karnauskas, 2017, Cowtan & Wei 2004) reflecting the Walker Circulation with both PHYDA-WPG reconstructions (Fig. 2; **Figs. S4**). In general, we observed a stable relationship with WPG_{obs}, Niño3.4, ZG_{sst} and ZG_{slp} between 1880 and 2000 with lowest correlations pre-1880 (**Figs. S2**). The latter is most probably due to sparse observations pre-1880 with higher uncertainties in instrumental data (results for PWPG-C are similar, see **Fig. S3**). The WPG_{obs}, Niño3.4 and ZG_{sst} are consistent with each other showing stable relationships throughout the record with a breakdown pre-1880 (Figs. 2 and 3; **Figs. S2 and S3**). The WPG_{obs} also displayed a stable relationship with the zonal SLP gradient mirroring the relationship shown by the PHYDA WPG's (**Figs. S5**). Other ENSO

reconstructions display significant relationships with the ZG_{sst} and ZG_{slp}, yet less stable than both PHYDA WPGs (**Fig. S6**).

Having established that the reconstructed PWPG-HF and PWPG-C reflect stable relationships for the instrumental data period, we now consider the full Last Millennium reconstruction of the WPG and Niño3.4. Both, PHYDA WPGs are nearly identical with slight amplitude differences (Figs. 2a, c; Fig. 3a; **Fig. S7**). Both WPG reconstructions also co-vary with the ZG_{sst} and Niño3.4 from PHYDA, again with slight differences in absolute magnitudes (Figs. 2a, c; Fig. 3b; **Fig. S7**). There is no long-term trend in both WPGs, yet significant interannual to multidecadal variability (Figs. 2 and 3). Most of the 11th century was dominated by a positive WPG and Niño3.4 (negative ZG_{sst}) with a switch to negative WPG and Niño3.4 (positive ZG_{sst}) towards the late 11th century. Between 1100 and 1300 A.D., neutral or weak positive WPG conditions alternated with moderate to strong negative WPG. The early 14th century experienced strong positive WPGs followed by strong negative WPGs (positive ZG_{sst}) in the mid 14th century and around 1400 A.D.. Between 1400 A.D. and 1600 A.D. negative WPG and Niño3.4 anomalies (positive ZG_{sst}) dominated with intermittent weak to moderate positive WPG periods (negative ZG_{sst}). The early 1600s have seen individual strong positive WPG (negative ZG_{sst}) years followed by a period of weakly positive WPG years alternating with moderate to strong negative WPG conditions. The mid-1700s showed a brief period of extreme WPG swings from strongly positive to strongly negative WPG (similar for ZG_{sst}). During the early to mid 1800s the ZG_{sst} agrees better with PWPG-C than with PWPG-HF (Fig. 2a, c) with the ZG_{sst} (positive PWPG-C) on average in a negative mean state while PWPG-HF shows only moderate swings from positive to negative. The early and late 19th century experienced strong negative WPGs (positive ZG_{sst}) while the early and late 20th century was dominated by both strong positive and negative WPG conditions (similar for ZG_{sst}) with weaker variability in the mid-20th century.

Both reconstructed WPGs also compared well with palaeo-Niño3.4 indices by Emile-Geay et al. (2013a, b; herafter Niño3.4 EG13) starting in 1150 A.D. and McGregor et al. (2010; hereafter MG10; Fig. 3c, e; **Figs. S7 and S8**) starting in 1650 A.D. The palaeo-Niño3.4 indices by Emile-Geay et al. (2013a, b) also co-varies with the PHYDA Niño3.4 based reconstruction (Fig. 3d; **Fig. S7 and S8**). However, differences in absolute magnitudes and sign were observed with the palaeo-Niño3.4 EG13, for instance around 1150 A.D., 1400 A.D. and during the late 16th, early 17th and 18th centuries. With MG10, the interannual and decadal variability is well matched to both PHYDA WPGs, yet the absolute magnitude was higher in MG10 for individual years or events (Fig. 3e; **Fig. S7 and S8**). The stability of relationships between our PHYDA WPGs and Niño3.4 reconstructions with the palaeo-Niño3.4 EG13 and MG10 indices was confirmed by 31-year running correlations (**Fig. S8**). Our analysis suggested that the relationship was stable for most of the record with multidecadal periods of weakening correlations (Fig. 2; **Fig. S7 and 8**). Interestingly, one of those periods was around the mid-19th century. Other periods with weaker relationships include the 13th, 15th and late 18th century (Fig. 3; **Fig. S7 and 8**). We also compared our WPGs with a recent reconstruction of ENSO flavors from coral proxy data (Freund et al., 2019) going back to 1620 A.D. to take into account temporally shifting centres of action for ENSO (**Fig. S9**). We found tight relationships during the 20th century with both the cold tongue index (NCT) and central Pacific ENSO (NWP) indices (**Fig. S9**),

stronger with the NCT. The early and mid-19th century showed weakening correlations with both NCT and NWP. Correlations with the NWP were strong around 1750, while those with the NCT were weak. Around 1700 the NCT (NWP) showed stronger (weaker) with both PHYDA WPG's while pre-1700 both NWP and NCT showed weak to moderately strong relationships (**Fig. S9**). We also assessed the relationship of the paleo-Niño3.4 EG13 and UEP MG10 with observed Niño3.4, as well as the zonal SST and SLP indices (**Fig. S10**). MG10 UEP and Niño3.4 EG13 indicate relatively stable relationships with observed Niño3.4 and zonal SST/SLP gradients pre-1960 with a weakening post-1960 (**Figs. S5**) while the PHYDA Niño3.4 reconstruction showed stable correlations for the entire record (**Fig. S2 and 3**).

In order to extract the occurrence of extreme positive WPG and negative WPG periods across the last Millennium we grouped the extreme events, calculated as the 90th percentile of standardized indices, in our reconstructions and the observed WPG (Fig. 4). This analysis revealed the co-occurrence of extreme negative WPG and Niño3.4 anomalies during the early and late 12th century, around 1400 A.D. and between 1400-1600s and several other shorter periods, as does the co-occurrence of extreme positive WPG and Niño3.4 anomalies in the early 11th century and the 20th century. The late 16th to early 17th century period were characterized by a warmer western then central Pacific with more negative WPGs well above the 20th century magnitude for strong negative WPG and Niño3.4. The Medieval Climate Anomaly (1100–1400 A.D.) was dominated by multidecadal swings of positive and negative WPG and Niño3.4 anomalies with a slight skewness towards higher amplitude negative WPG conditions compared to fewer high magnitude positive WPG. This is in agreement with Goodwin et al., (2014) who found a multidecadal dominance of EP La Nina and CP La Nina during the MCA. During the colder 18th and 19th centuries in the Western Pacific, the occurrence between positive and negative WPG was more balanced with a dominance of interannual variability. The 20th century indicated an unprecedented cluster of frequent co-occurrences of both extreme negative WPG and Niño3.4 and extreme positive WPG and Niño3.4 anomalies. We assessed changes in WPG variability through 51-year running standard deviations in both PHYDA WPGs, as well as PHYDA Niño3.4 and Niño3.4 EG13 over the full length of records (**Fig. S11**). The 20th century showed the most extreme variability over the Last Millennium with equally strong positive and negative WPG and Niño3.4 anomalies (Fig. 4; **Fig. S11**). However, the diminishing quantity of proxy data in the early part of the Last Millennium calls for caution when inferring changes in variance between the modern period and distant past. The Niño3.4 EG13 index mostly agrees with our results based on WPG reconstructions in showing highest variability in the 20th century and enhanced standard deviations in the early 13th, the 16th and early 17th centuries (**Fig. S11**).

The question arises if these changes in mean state and their variability had influenced rainfall-drought cycles in global hydrology. To answer this question, we first verified if the reconstructed WPG does reproduce the observed relationships with SST, SLP and rainfall across known ENSO impacted regions. Figure 5 illustrates that our PWPG-HF index reproduced the expected spatial correlations as does the observed WPG. Strongest relationships were found with SST and SLP across the Indo-Pacific Ocean and rainfall in Eastern Australia, the Maritime Continent, the Indian Monsoon region, SW US and the dipoles between North and South America and East and South Africa. Subsequently, we have contrasted our WPG time series with those of long-term hydrological reconstructions. We used the drought atlases for

Australia and New Zealand (ANZDA; Palmer et al., 2015), the North American Drought Atlas (NADA; Cook et al., 1999, 2008, 2016) and South American Drought Atlas (SADA; Morales et al., 2020) as examples (Fig. 5c-e; **Fig. S12 and S13**). Figure 5 illustrates that our PWPG-HF index co-varied positively with the NADA (SW US) and SADA grid boxes for central Chile, while it is negative with the ANZDA grid box for eastern Australia. The multidecadal oscillation of dry and wet periods observed in NADA between 1200 and 1600 and 1850 to present were mirrored by our WPG indices (Fig. 5c). The extreme multidecadal NADA droughts around 1400 and in the late 16th to early 17th century was clearly associated with a series of extreme negative WPG and Niño3.4 anomalies (Fig. 5c). The ANZDA time series revealed that positive WPG and Niño3.4 conditions were associated with dry anomalies in eastern Australia and vice versa for wet periods (Fig. 5d). The South American record from central Chile displayed an association of wet periods with positive WPG and Niño3.4 and vice versa for dry periods (Fig. 5e). Again, the late 16th century indicated dry anomalies with strong negative WPGs and Niño3.4 anomalies.

Discussion

We have shown that the WPG during ENSO is a novel index for Last Millennium Walker Circulation strength, the latter defined by SST and SLP gradient indices across the tropical Pacific (Karnauskas et al., 2009; Tokinaga et al., 2012; Coats & Karnauskas, 2017; L'Heureux et al., 2013). For the 20th century, we also show that the WPG captured the SST and precipitation teleconnection patterns qualitatively similar to ENSO and Walker Circulation indices. Compared to other paleo-ENSO indices (Emile-Geay et al., 2013a, b; McGregor et al., 2010), the WPG showed a more stable relationship with the observed PWC indices (Coats and Karnasukas, 2017). Thus, the WPG is a key index for the PWC in the instrumental era and also for the past Millennium. We did not observe a clear linear trend in the WPG during the Last Millennium. Instead, both Last Millennium WPGs and ZG_{sst} showed multi-decadal to multi-centennial variability with more negative WPG and La Niña or CP La Niña-like occurrences (positive ZG_{sst}) in the late 11th, mid-late 12th, at the turn of the 14th century, between 1400-1600s, mid 1700s and since 1870 (West Pacific warmer than the central Pacific). Positive WPG and El Niño or CP El Niño-like occurrences (negative ZG_{sst}) dominated the first century of the Last Millennium, the early 14th and short periods in the 11th and 18th centuries (West Pacific colder than central Pacific). The 20th century stands out as period with both strong positive and negative WPG (and ZG_{sst}) occurrences and overall highest variability (running standard deviations) over the past Millennium. However, several studies caution oversimplified interpretations of variance changes due to diminishing proxy availability over time (Comboul et al., 2014; Dee et al., 2020). Nevertheless, our results are largely in agreement with other Niño3.4 indices in terms of multi-decadal oscillations and changing variance over time, despite vastly different methodologies (Abram et al., 2020; McGregor et al., 2010; Emile-Geay et al., 2013; Steiger et al., 2019). Clearly, the WPG could be an excellent index for CP ENSO or Modoki phases which often are characterized by strong SST gradients between the western and central Pacific, yet same sign anomalies in the EP and for the WP. Hoell and Funk (2013) showed evidence that most negative WPG phases since 1950 were associated with central Pacific or La Niña Modoki events while positive WPG phases had an affinity to occur predominantly during eastern Pacific or canonical ENSO events. However, a number of positive or

negative WPG phases were associated with mixed type ENSO flavors. Thus, periods of extreme negative WPG in our Last Millennium reconstructions may represent La Niña or La Niña Modoki conditions, while positive WPG periods may indicate EP El Niño or mixed CP and EP El Niño flavors. To assess the relationship between ENSO flavors and the WPG, we turned to the NCT and NWP reconstructions based on Pacific coral proxy records (Freund et al., 2019; Figs. 3 and S8). The NWP and NCT study considered El Niño flavors only, yet the index also includes the La Niña flavors. Our hypothesis was that the NWP should predominatly co-vary with the WPG positive (negative) events when the latter would predominatly reflect Modoki or CP El Niño (CP La Niña) events. The comparison of the WPG indices with the NCT (EP) and NWP (CP) ENSO flavor indices revealed time varying relationships, especially between 1600 and 1850, yet strongest co-variability with both since the mid-19th century to the present (Freund et al., 2019; Fig. S8). The relationship during the mid/end-18th century revealed closer agreement with the NWP (CP flavor) while the early 18th century WPG indicated closer alignement with the NCT (EP flavors). However, the 18th century is also known for its reduced proxy data coverage in the Pacific Ocean, so should be viewed with caution (Freund et al., 2019). The enhanced CP to EP event ratio during the 17th century is less clearly reflected by the WPG's. The WPG's do, however, indicated extreme negative events (positive ZG_{sst}) in the early and late 17th century (Figs. 2 and 3). However, when taking into account centennial mean state changes (without detrending), the WPG appears to reflect dominantly negative WPG or La Niña Modoki conditions with the exception of the 11th and 20th centuries, the early 14th and early 18th centuries and several short-lived periods over the past Millennium (Fig. 2). Thus, during the last Millennium the WPG mean state changes appeared to have skewed the WPG towards La Niña or La Niña Modoki type events for most of the time. Thus, there appears to a relationship between Pacific SST mean state, ZG_{sst} and the WPG.

We also established the hydroclimatic relationships of the WPG with the three drought atlases which were largely in agreement with assessments of ENSO impacts on drought and pluvial conditions. In accordance with the findings of Steiger et al. (2019), megadroughts in southwestern North America were found to be associated with an extremely negative WPG (positive ZG_{sst}) and colder values of the Niño3.4 index in PHYDA. The North American megadroughts around 1400 and the turn of the 16th to 17th century during the Little Ice Age stand out as periods with persistent negative WPG and Niño3.4 anomalies (positive ZG_{sst}). The latter is consistent with Dee et al. (2020) and Steiger et al. (2019) who showed evidence for enhanced North America ENSO teleconnections during the Little Ice Age. The latter was found to hold for both El Niño and La Niña events and was shown to be unaffected by proxy availability over time. In other words, we find more drying in the North American Southwest in more negative WPG years (positive ZG_{sst}) during periods of enhanced ENSO teleconnections. Steiger et al. (2019) pointed out that the megadroughts pre-1600 were likely radiatively unforced and most strongly associated with unusually cold SST in the central and eastern Pacific and warm SST in the Atlantic. Yet, they also showed evidence for a potential role of local radiative forcing in excerbating regional drought in the North American Southwest. The western Pacific region of the WPG and MC are oceanic regions of high sensitivity to radiative forcing (Funk & Hoell, 2015; Chung et al., 2019; Seager et al., 2019). Thus, changes to the WPG might bear a footprint of local radiative forcing coupled with slow decadal oceanic feedbacks

that affect the SST patterns in the Pacific and associated teleconnections (Luo et al., 2017). Thus, the SST patterns across the western Pacific appear to play a crucial role in the drought inducing teleconnections in addition to those in the central and eastern Pacific.

ENSO was also shown to play an important role in South American hydroclimate next to SAM and Atlantic influences (Morales et al., 2020). Wet conditions were found during positive Niño3.4 anomalies in southeastern South America and central Chile while dry conditions prevailed during negative Niño3.4. The PHYDA WPG reconstructions revealed that wet conditions persisted in central Chile during a positive WPG while dry conditions prevailed during the negative WPG phases. This is largely in agreement with ENSO teleconnections based on the SADA (Morales et al., 2020). Our study suggested a weaker influence of the WPG on central Chile in parts of 18th and 19th centuries. Here, influences from the SAM or Atlantic could have a played a larger role.

Eastern Australia was shown to experience wetter condition during La Niña phases and drier conditions during El Niño phases amplified by negative and positive Interdecadal Pacific Oscillation (IPO) phases, respectively (Palmer et al., 2015). Our WPG reconstruction revealed three periods of negative correlations with the Eastern Australia region in ANZDA during the turn of 16th to 17th century, between 1700–1800 and the 20th century. Weaker relationships with the WPG were observed in between. The WPG also showed the typical anti-correlation between Eastern Australia and southern New Zealand PDSI in ANZDA between 1500 and 2000 AD (Palmer et al., 2015; Fig. S13). The relationship during the 20th century indicated that teleconnections with the WPG were strongest when ENSO variability was higher between 1880–1920 and since 1960. The latter is consistent with abundant evidence from previous studies of enhanced ENSO teleconnections during strong ENSO phases (Torrence and Compo, 1998; Mestas-Nunez and Enfield, 2001; Wang et al., 2019). ENSO modulation by low-frequency oscillations of the IPO can modulate ENSO impacts on Australia (Verdon et al., 2004; McGovan et al., 2009). The latter may also hold for relationships between Eastern Australia PDSI in ANZDA and the WPG.

In summary, the new PHYDA WPG reconstructions indicated robust hydroclimate teleconnections with regions sensitive to ENSO and WPG drought and pluvial conditions across the Pacific and on its rims. The late 16th century was confirmed as period of strong negative WPG, positive ZG_{sst} and Niño3.4 occurrences with megadroughts in North America and South America and pluvials in Australia. This illustrates that the WPG may serve as a powerful index together with ENSO indices to reveal the impact of drought-inducing climate teleconnections that arose from changes in Pacific SST patterns. We call for a concerted effort of generating new proxy data from this key region in the western Pacific which could dramatically improve the knowledge base for centennial and decadal PWC changes.

Methods

WPG temperature variability over the past millennium is reconstructed using the Paleo Hydrodynamics Data Assimilation (PHYDA; Steiger et al., 2018; https://zenodo.org/record/1198817#.YGXM4khKjUI). PHYDA is analogous to modern reanalysis products but constrained by paleoclimate data instead of

meteorological observations (Hakim et al., 2016; Steiger et al., 2018). PHYDA uses data assimilation of multivariate palaeoclimate proxy data with the dynamical constraints of a Last Millennial Ensemble simulations, the Community Earth System Model Ensemble (CESM LME; Otto-Bliesner et al., 2015). The PHYDA approach preserves dynamical relationships between ocean and atmospheric variables and accommodates periods of non-stationary teleconnections. PHYDA uses 2978 annually-resolved proxy records, which builds on the PAGES2k proxy network (PAGES Consortium 2017). PHYDA reconstructions of gridded 2m temperature at 2 degree spatial grid resolution for annual means were accessed for this work. PHYDA derived climate parameters were extensively validated against instrumental observations in Steiger et al. (2018). We calculated all climate indices from PHYDA at annual resolution since 1000 AD.

The WPG temperature has been calculated using the Hoell & Funk (2013) and Cai et al. (2015) approaches from PHYDA. The WPG was originally defined by Hoell and Funk (2013) as the standardized difference between the central Pacific (Niño4 region; 5°S-5°N, 160–210°E) and western Pacific SST (0–10°N, 130–150°E) between 1854 and 2010 from ERSSTv3b (Smith et al., 2008). The WPG_{Obs} (based on Hoell & Funk, 2013) from observations relies on a similar 2º spatial grid resolution as PHYDA. Cai et al. (2015) calculated an air temperature gradient between the Niño4 region (5S-5N, 160E-150W) and the Maritime continent region (5S-5°N, 100–125°E). Here, we apply both definitions and extracted the relevant temperature data from the gridded data in PHYDA defining both WPG definitions by subtracting the annual PHYDA-derived SST for the western Pacific boxes defined by Hoell and Funk (2013) and Cai et al. (2015) from Niño.4 SST. We used the range of uncertainties provided in the original PHYDA data (Steiger et al., 2018) to assess uncertainty ranges in our WPG reconstruction (Fig. S14 and S15).

We validated the PHYDA based time series of the WPG, Niño3.4 and Niño.4 indices with temporal and spatial field correlations with the observed WPG from COBE2 SST (Hirahara et al., 2014), instrumental ENSO indices (Kaplan et al., 1998), Walker Circulation indices for SST and SLP (Coats & Karnauskas, 2017; L'Heureux et al. 2013), GPCC gridded rainfall station (Schneider et al., 2013) and 20th century reanalysis rainfall data (Slivinski et al., 2019).

Several palaeoclimate indices for ENSO were used to verify the PHYDA Niño3.4 and WPG based indices beyond the coverage of observational data. These include the Niño3.4 index of Emile-Geay et al. (2013) and the Unified ENSO Index (UEP) from McGregor et al. (2010). Walker Circulation variability was based on indices of zonal differences in sea level pressure (SLP) and SST for grid boxes defined in Coats & Karnauskas (2017) and L'Heureux et al. (2013).

We extracted Palmer Drought Severity Indices (PDSI) from the drought atlases for Australia and New Zealand (ANZDA; Palmer et al., 2015), the North American Drought Atlas and American Southwest (NADA; Cook et al., 1999, 2008) and South American Drought Atlas (SADA; Morales et al., 2020).

Spatial correlations between physical climate data and PHYDA were computed in KNMI climate explorer (Trouet & Oldenborgh, 2013). Only correlations > 95% significance were considered. 31-year and 51-year running correlations were also computed in KNMI climate explorer using detrended annual means with

statistical significance > 95% level computed against a 1000 sample Monte Carlo simulation. The 95% confidence interval was computed for all running correlations. Extreme WPG and ENSO events were calculated based on 90th percentile of standardized indices.

All data generated for the West Pacific Gradient and zonal sea surface temperature gradient from PHYDA will be made available on the NOAA Paleoclimate data server (https://www.ncdc.noaa.gov/data-access/paleoclimatology-data).

Declarations

Acknowledgements

We like to acknowledge the PAGES2k community and the Paleo Hydrodynamics Data Assimilation product developers for open access to all palaeoclimate data. JZ was supported by a Royal Society Wolfson Fellowship. AH was supported by NOAA's Climate Program Office's Modeling, Analysis, Predictions, and Projections Program, Grant #V8R1CA7-P04.

References

1. Abram, N. J. *et al.* & D. Heslop Coupling of Indo-Pacific climate variability over the last millennium. *Nature.* **579**, 385–392 (2020).
2. Allan, R. J., Nicholls, N., Jones, P. D. & Butterworth, I. J. A further extension of the Tahiti-Darwin SOI, early SOI results and Darwin pressure. *J. Climate.* **4**, 743–743 (1991).
3. Annamalai, H., Hafner, J., Sooraj, K. P. & Pillai, P. Global Warming Shifts the Monsoon Circulation, Drying South Asia.Journal of Climate26 (9),2701–2718.
4. Bothe, O., Jungclaus, J. H. & Zanchettin, D. Consistency of the multi-model CMIP5/PMIP3-past1000 ensemble. *Clim Past.* **9**, 2471–2487 (2013).
5. Cai, W. *et al.* Increased frequency of extreme La Niña events under greenhouse warming. *Nature Climate Change.* **5**, 132–137 (2015).
6. Chung, E. S. *et al.* Reconciling opposing Walker circulation trends in observations and model projections. *Nature Climate Change.* **9**, 405–412 (2019).
7. Cook, E. R. *et al.* Megadroughts in North America: placing IPCC projections of hydroclimatic change in a long-term palaeoclimate context. *Journal of Quaternary Science.* **25**, 48–61 (2010).
8. Coats, S., Smerdon, J. E., Cook, B. I. & Seager, R. Are simulated megadroughts in the North American Southwest forced? *J Clim.* **28**, 124–142 (2015).
9. Coats, S. *et al.* Internal ocean-atmosphere variability drives megadroughts in Western North America. *Geophys. Res. Lett.* **43**, 9886–9894 (2016).
10. Coats, S. & Karnauskas, K. B. Are Simulated and Observed Twentieth Century Tropical Pacific Sea Surface Temperature Trends SignificantmRelative to Internal Variability? *Geophysical Res. Lett.* **44**,

9928–9937 (2017).

11. Comboul, M. *et al.* A probabilistic model of chronological errors in layer-counted climate proxies: applications to annually banded coral archives. *Climate of the Past.* **10**, 825–841 (2014).
12. Compo, G. P. & Sardeshmukh, P. D. Removing ENSO-Related variations from the climate record. *J. Climate.* **23**, 1957–1978 (2010).
13. Conroy, J. L., Overpeck, J. T., Cole, J. E. & Steinitz-Kannan, M. Variable oceanic influences on western North American drought over the last 1200 years. *Geophys. Res. Lett.* **Vol. 36**, L17703 https://doi.org/10.1029/2009GL039558 (2009).
14. Cook, E. R., Meko, D. M., Stahle, D. W. & Cleaveland, M. K. Drought reconstructions for the continental United States. *Journal of Climate.* **12**, 1145–1162 (1999).
15. Cook, E. R. & Krusic, P. J. North American summer PDSI reconstructions, Version 2a. IGBP PAGES/World Data Center for Paleoclimatology Data Contribution Series No. 2008-046, NOAA/NGDC Paleoclimatology Program, Boulder, CO(2008).
16. Cook *et al.* North American megadroughts in the Common Era: reconstructions and simulations. *Clim Change.* **7**, 411–432 (2016).
17. Cowtan, K. & Way, R. G. Coverage bias in the HadCRUT4 temperature series and its impact on recent temperature trends. *Quaterly Journal of the Royal Meteorological Society.* **140**, 1935–1944 (2014).
18. Dee, S., Okumura, Y., Stevenson, S. & Di Nezio, P. (2020). Enhanced North American ENSO teleconnections during the Little Ice Age revealed by paleoclimate data assimilation.Geophysical Research Letters, 47, e2020GL087504.
19. Emile-Geay, J., Cobb, K. M., Mann, M. E. & Wittenberg, A. T. Estimating tropical Pacific SST variability over the past millennium. Part 1: Methodology and validation. *J. Climate.* **26**, 2302–2328 (2013a).
20. Emile-Geay, J., Cobb, K. M., Mann, M. E. & Wittenberg, A. T. Estimating tropical Pacific SST variability over the past millennium. Part 2: Reconstructions and uncertainties. *J. Climate.* **26**, 2329–2352 (2013b).
21. Feng, M. *et al.* Decadal increase in Ningaloo Niño since the late 1990s. *Geophysical Res. Lett.* **41**, https://doi.org/10.1002/2014GL062509 (2015).
22. Freund, M. B. *et al.* Higher frequency of Central Pacific El Nino events in recent decades relative to past centuries. *Nature Geoscience.* **6**, 450–455 (2019).
23. Funk, C. & Hoell, A. The Leading Mode of Observed and CMIP5 ENSO-Residual Sea Surface Temperatures and Associated Changes in Indo-Pacific Climate. *Journal of Climate.* **28**, 4309–4329 (2015).
24. Goodwin, I. D., Browning, S. & Anderson, A. Climate windows for Polynesian voyaging to New Zealand and Easter Island. *P.* **Natl. A. Sci., 111**, 14716–14721 (2014). **)**
25. Griffin, D. & Anchukaitis, K. J. How unusual is the 2012–2014 California drought? Geophys. *Res. Lett.* **41**, 9017–9023 (2014).

26. Hakim, G. J. *et al.* The last millennium climate reanalysis project: Framework and first results. *J. Geophys. Res. Atmos.* **121**, 6745–6764 (2016).
27. Hirahara, S., Ishii, M. & Fukuda, V. Centennial-Scale Sea Surface Temperature Analysis and Its Uncertainty. *Journal of Climate.* **27**, 57–75 (2014).
28. Hoell, A. & Funk, C. The ENSO-related West Pacific Sea surface temperature gradient. *J. Clim.* **26**, 9545–9562 (2013).
29. Hoell, A., Funk, C. & Barlow, M. La Nina diversity and Northwest Indian Ocean Rim teleconnections. *Clim. Dyn.* **43**, 2707–2724 (2014a).
30. Hoell, A., Funk, C. & Barlow, M.The regional forcing of Northern hemisphere drought
31. during recent warm tropical west Pacific Ocean La Nina events. *Clim. Dyn.* **42**, 3289–3311 (2014b).
32. Kaplan, A. *et al.* Analyses of global sea surface temperature 1856–1991. *J. Geophys. Res.* **103**, 567–589 (1998).
33. Karnauskas, K. B., Seager, R., Kaplan, A., Kushnir, Y. & Cane, M. A. Observed strengthening of the zonal sea surface temperature gradient across the equatorial Pacific Ocean. *Journal of Climate.* **22**, 4316–4321 (2009).
34. Krishnan, R. *et al.* Indian Ocean-Monsoon coupled interactions and impending monsoon droughts. *Geophys Res Lett.* **33**, L08711 https://doi.org/10.1029/2006GL025811 (2006).
35. L'Heureux, M. L., Lee, S. & Lyon, B. Recent multidecadal strengthening of the Walker circulation across the tropical Pacific. *Nature Climate Change.* **3** (6), 571–576 (2013).
36. Li, J. *et al.* Interdecadal modulation of El Niño amplitude during the past millennium. *Nature Climate Change.* **1**, 114–118 (2011).
37. Li, J. *et al.* El Niño modulations over the past seven centuries. *Nature Climate Change.* **3**, 822–826 (2013).
38. Lüning, S., Gałka, M. & Danladi, I. B. Theophilus Aanuoluwa Adagunodod, Fritz Vahrenholt Hydroclimate in Africa during the Medieval Climate Anomaly. *Palaeogeogr., Palaeoclimatol. Palaeoecol.* **495**, 309–322 (2018).
39. Luo, Y. Y., Lu, J., Liu, F. K. & Garuba, O. The Role of Ocean Dynamical Thermostat in Delaying the El Nino-Like Response over the Equatorial Pacific to Climate Warming. *J Climate.* **30**, 2811–2827 (2017).
40. Lyon, B., Barnston, A. G. & DeWitt, D. G. Tropical pacific forcing of a 1998–1999 climate shift: observational analysis and climate model results for the boreal spring season. *Clim. Dyn.* **43**, 893–909 (2014). **)**
41. Mann, M., Bradley, R. S. & Hughes, M. K. Multiscale Variability and Global and Regional Impacts, in: Long-term variability in the El Niño-Southern Oscillation and associated teleconnections, Cambridge Univ. Press, 357–412(2000).
42. McGowan, H. *et al.* Reconstructing annual inflows to the headwater catchments of the Murray River, Australia, using the Pacific decadal oscillation Geophys. *Res. Lett.* **36**, L06707–5 (2009).

43. McGregor, S., Timmermann, A. & Timm, O. A unified proxy for ENSO and PDO variability since 1650, Clim. *Past.* **6**, 1–17 (2010).
44. Mestas-Nuñez, A. M. & Enfield, D. B. Eastern equatorial Pacific SST variability: ENSO and non-ENSO components and their climatic associations. *J. Climate.* **14**, 391–402 (2001).
45. Morales, M. S. *et al.* Six hundred years of Soutrh American tree rings reveal an increase in severe hydroclimatic events since mid-20th century. *PNAS.* **117** (9), 16816–16823 (2020).
46. Neal, R. & Slingo, J. M. The Maritime Continent and its role in the global climate: a GCM study. *Journal of Climate.* **16**, 834–848 (2003).
47. Otto-Bliesner *et al.* 2015,B. Am. Meteorol. Soc., doi:10.1175/BAMS-D-14-00233.1
48. PAGES2k Consortium. A global multiproxy database for temperature reconstructions of the common era. *Sci. Data.* **4**, 170088 (2017).
49. Palmer, J. G. *et al.* Drought variability in the eastern Australia and New Zealand summer drought atlas (ANZDA, CE 1500–2012) modulated by the Interdecadal Pacific Oscillation. *Environmental Research Letters.* **10** (12), 124002 https://doi.org/10.1088/1748-9326/10/12/124002 (2015).
50. Pfeiffer, M. *et al.* Indian Ocean corals reveal crucial role of World War II bias for twentieth century warming estimates. *Sci. Rep.* **7**, 14434 https://doi.org/10.1038/s41598-017-14352-6 (2017).
51. Quian, J. H. Why Precipitation Is Mostly Concentrated over Islands in the Maritime Continent. *Journal of the Atmopsheric Sciences.* **65**, 1428–1441 (2008). **)**
52. Ratna, S. B. *et al.* Moisture variability over the IndoPacific region and its influence on the Indian summer monsoon rainfall. *Clim. Dyn.* **46**, 949–965 (2016).
53. Schneider, U. *et al.* GPCC's new land surface precipitation climatology based on quality-controlled in situ data and its role in quantifying the global water cycle. *Theoretical and Applied Climatology.* **115**, 15–40 (2013).
54. Seager, R. *et al.* Strengthening tropical Pacific zonal sea surface temperature gradient consistent with rising greenhouse gases. *Nature Climate Change.* **9**, 517–522 (2019).
55. Smith, T. M., Reynolds, R. W., Peterson, T. C. & Lawrimore, J. Improvements to NOAA's Historical Merged Land-Ocean Surface Temperature Analysis (1880–2006). *J. Climate.* **21**, 6472283–6472296 (2008).
56. Solomon, A. & Newman, M. Reconciling disparate twentieth-century Indo-Pacific ocean temperature trends in the instrumental record. *Nature Climate Change.* **2**, 691–699 (2012).
57. Slivinski, L. C. *et al.* (2019), Towards a more reliable historical reanalysis: Improvements for version 3 of the Twentieth Century Reanalysis system. Q J R Meteorol Soc. 145, 2876–2908 (2019).
58. Stahle, D. *et al.* Experimental dendroclimatic reconstruction of the Southern Oscillation. *B. Am. Meteorol. Soc.* **79**, 2137–2152 (1998).
59. Steiger, N. J., Smerdon, J. E., Cook, E. R. & Cook, B. I. Data Descriptor: A reconstruction of global hydroclimate and dynamical variables over the Common Era.Sci Data5, (2018).

60. Steiger, N. J. *et al.* Oceanic and radiative forcing of medieval megadroughts in the American Southwest. *Sci. Adv.* **5** (7), eaax0087 (2019).
61. Tierney, J. E., Ummenhofer, C. C. & deMenocal, P. B. 2015. Past and future rainfall in the Horn of Africa.Science Advances1.
62. Tokinaga, H., Xie, S. P., Deser, C., Kosaka, Y. & Okumura, Y. M. Slowdown of the Walker circulation driven by tropical Indo-Pacific warming. *Nature.* **491**, 439–443 (2012).
63. Torrence, C. & Compo, G. P. A practical guide to wavelet analysis. *Bull. Amer. Met. Soc.* **79** (1), 62–78 (1998).
64. Trouet, V. & van Oldenborgh, G. J. KNMI Climate Explorer: a web-based research tool for high-resolution paleoclimatology. *Tree-Ring Res.* **69**, 3–14 (2013).
65. Kataoka, T., Tozuka, T., Behera, S. & Yamagata, T. On the origin of Ningaloo Nino/Nina. *Clim. Dyn.* **43** (5–6), 1463–1482 (2014).
66. Verschuren, D., Laird, K. R. & Cumming, B. F. Rainfall and drought in equatorial east Africa during the past 1,100 years. *Nature.* **403**, 410–414 (2000).
67. Verdon, D. C., Wyatt, A. M., Kiem, A. S. & Franks, S. W. Multidecadal variability of rainfall and streamflow: Eastern Australia Water Resour. *Res.* **40**, W10201 https://doi.org/10.1029/2004WR003234 (2004).
68. Wang, B. *et al. J. Historical change of El Niño properties sheds light on future changes of extreme El Niño. PNAS.* **116**, 22512–22517 (2019).
69. Wilson, R. *et al.* Reconstructing ENSO: the influence of method, proxy data, climate forcing and teleconnections. *J. Quat. Sci.* **25**, 62–78 (2010).
70. Zinke, J. *et al.* Coral record of southeastern Indian Ocean marine heatwaves with intensified Western Pacific temperature gradient. *Nature Communications.* **6**, https://doi.org/10.1038/ncomms9562 (2015).

Figures

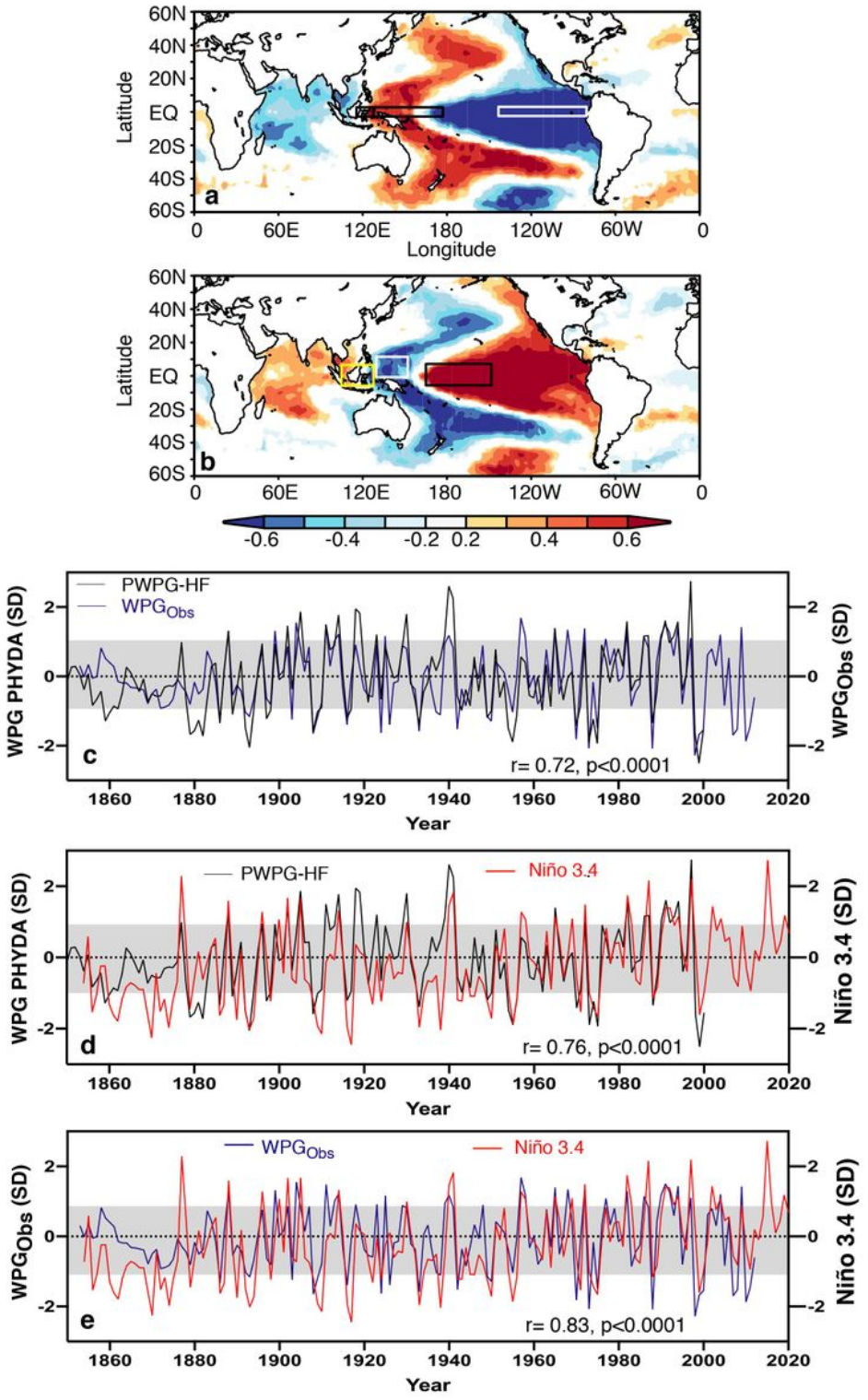

Figure 1

Zonal Pacific SST gradient (COBE2; Hirahara et al; 2014) and West Pacific gradient (WPG; Hoell and Funk, 2013) correlation with HadISST (Compo et al., 2011) and WPG PHYDA reconstruction. a) Zonal SST gradient from COBE2 (Hirahara et al., 2014) following definition of Coats & Karnauskas 2017 (SST difference between 2.5°N-S, 117°E–173°E and 2.5°N-S, 205°E–275°E; see rectangular boxes) correlated with HadISST and b) WPG following definition of Hoell & Funk (2013) correlated with HadISST (black and

white box= WPG Hoell & Funk, 2013; yellow and white box= WPG Cai et al., 2015). Spatial correlations computed in knmi climate explorer, only correlation at 95% level coloured (Trouet & Oldenborgh, 2013). PHYDA-West Pacific Gradient (WPG) reconstruction with 1 SD (grey bar) compared with c) observed WPG after Hoell & Funk (2013) based on ERSSTv3b and d) observed Niño3.4 index (Kaplan et al., 1998) and e) observed WPG after Hoell & Funk (2013) based on ERSSTv3b and observed Niño3.4 index (Kaplan et al., 1998). Correlation coefficients are indicated over full period of overlap for detrended data.

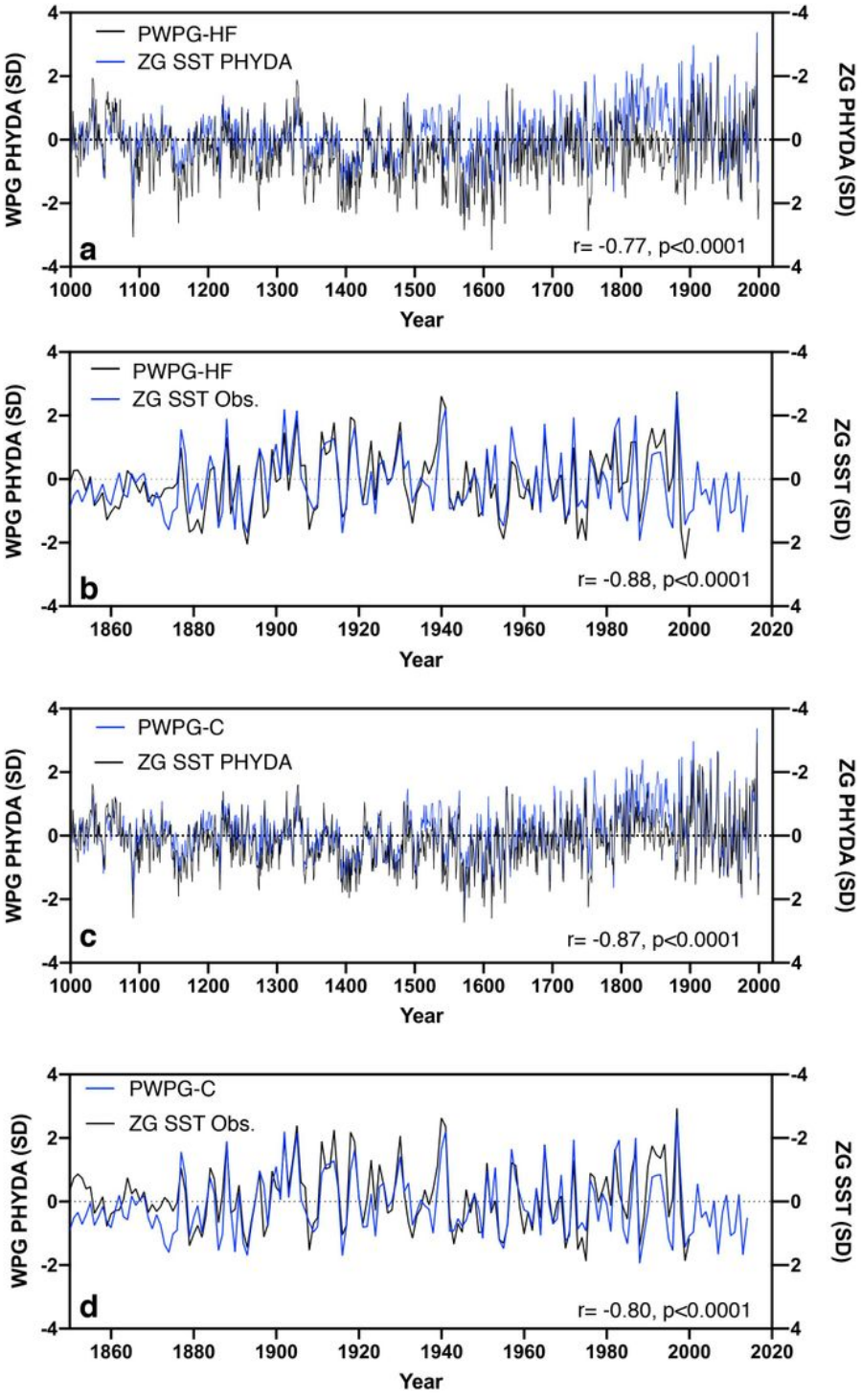

Figure 2

Reconstructed and Observed zonal (West – East) Pacific SST Gradient compared to West Pacific Gradient (WPG) reconstructions. PWPG-HF reconstruction compared with a) PHYDA zonal SST gradient after Coats & Karnauskas (2017), b) observed zonal SST gradient from COBE2 SST (axis inverted; Hirahara et al., 2014) after Coats & Karnauskas (2017). PWPG-C reconstruction compared with c) PHYDA zonal SST gradient after Coats & Karnauskas (2017) and d) observed zonal SST gradient after Coats & Karnauskas (2017) from COBE2 SST (axis inverted; Hirahara et al., 2014). Correlation coefficients are indicated over full period of overlap for detrended data.

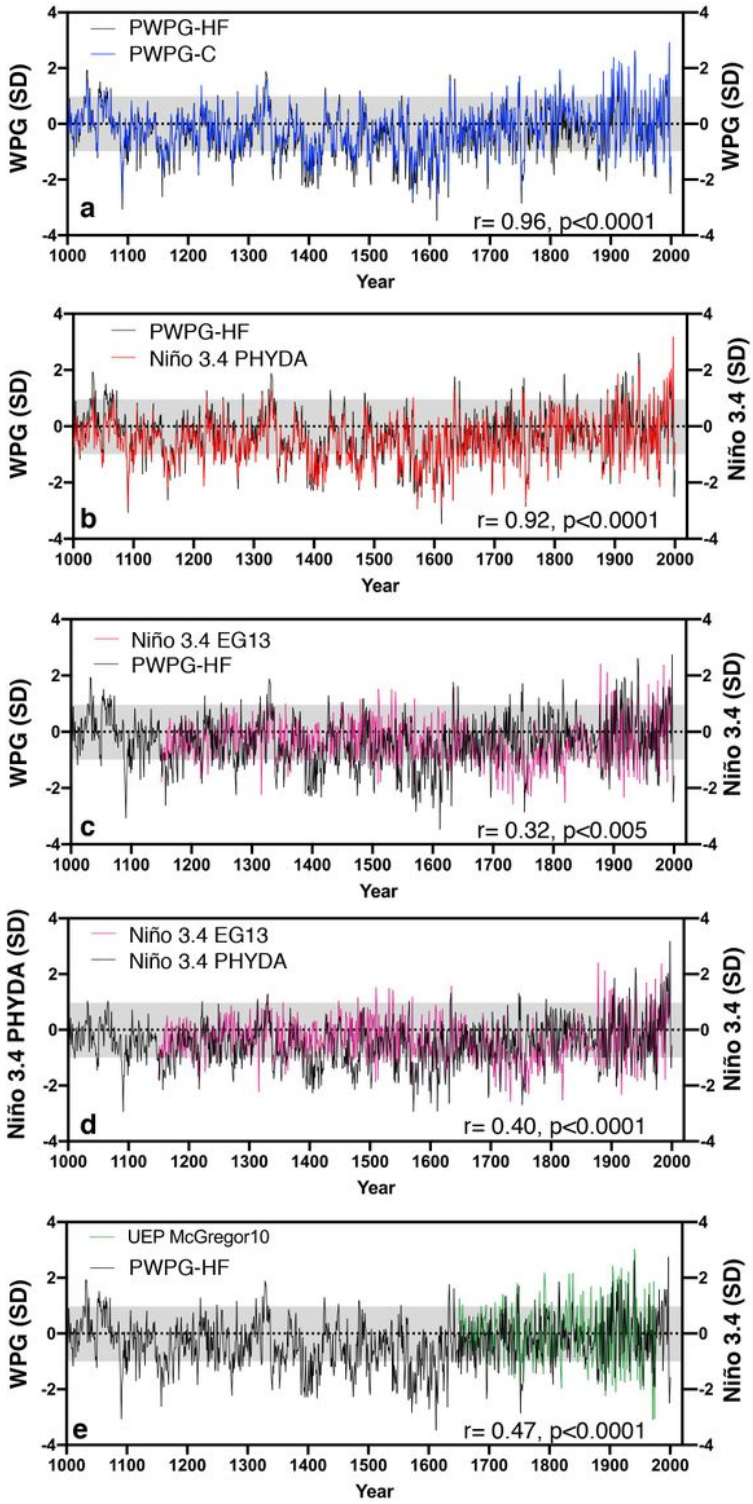

Figure 3

Mean annual reconstruction of the WPG from the Last Millennium PHYDA multivariate proxy network. WPG based on Hoell & Funk (2013; black line) with one standard deviation (SD; grey bar) threshold compared to a) WPG based on definition of Cai et al. (2015; blue), both calculated from PHYDA, b) PHYDA-based Niño3.4 index (red line), c) Niño3.4 reconstruction (magenta line) of Emile-Geay et al. (2013), d) PHYDA-based Niño3.4 index (black line) compared to Niño3.4 reconstruction (magenta line) of Emile-Geay et al. (2013) and e) the WPG based on Hoell & Funk (2013; black line) compared to the Niño3.4 reconstruction (green line) of McGregor et al. (2010). Correlation coefficients are indicated over full period of overlap for detrended data.

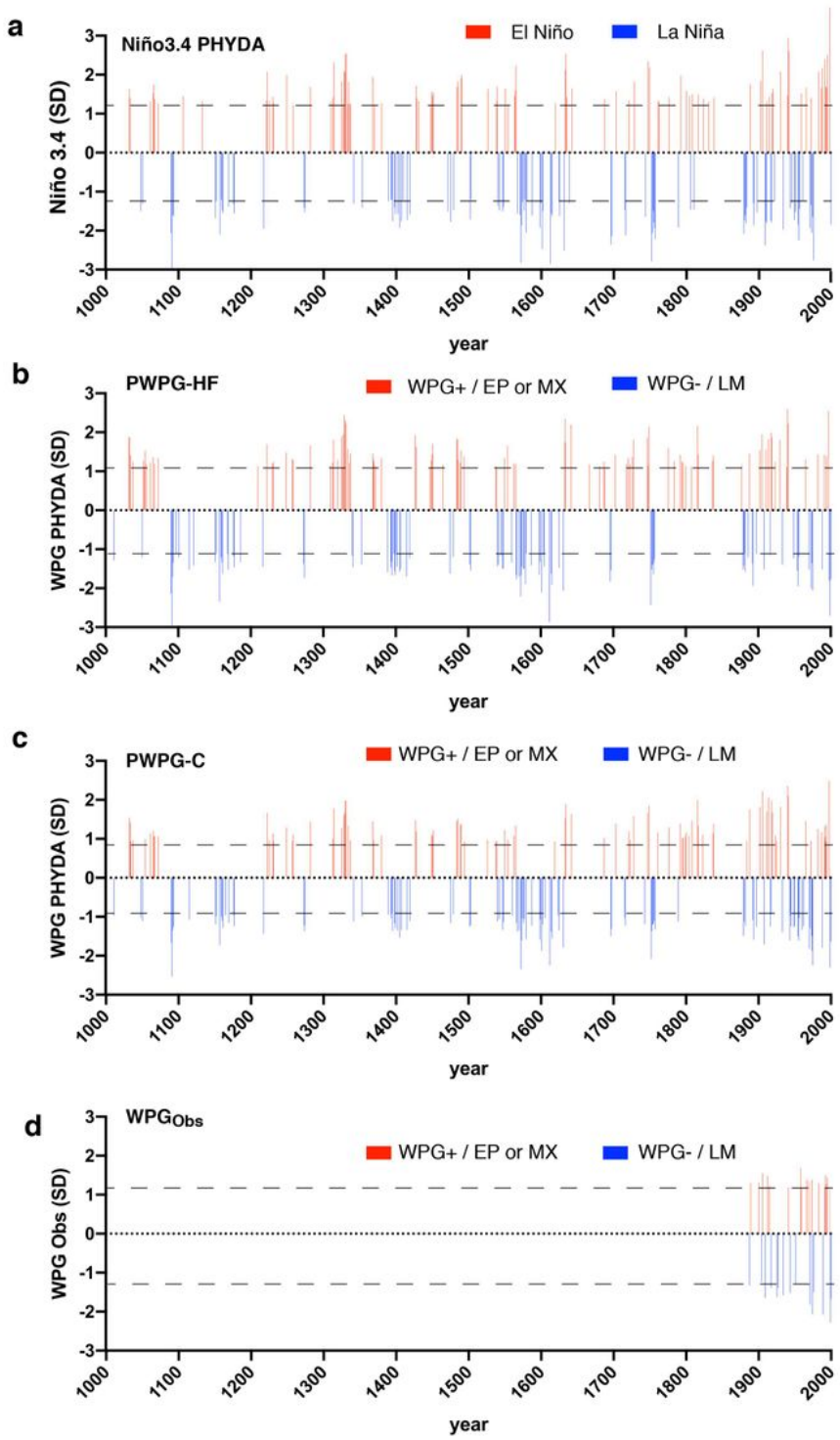

Figure 4

Extreme events based on 90th percentile of standardized and detrended indices. a) Niño3.4 index from PHYDA, b) PHYDA-WPG (PWPG-HF) based on Hoell & Funk (2013), c) PHYDA-WPG (PWPG-C) based on Cai et al. (2015), and d) observed WPG based on Hoell & Funk (2013). All positive (WPG+) and negative (WPG-) event thresholds >90% percentile unique to each index illustrated by dashed lines. Only events

that exceed the 90th percentile are shown. EP= eastern Pacific El Niño events, MX= mixed eastern-central Pacific El Niño events, LM= La Niña Modoki-type events.

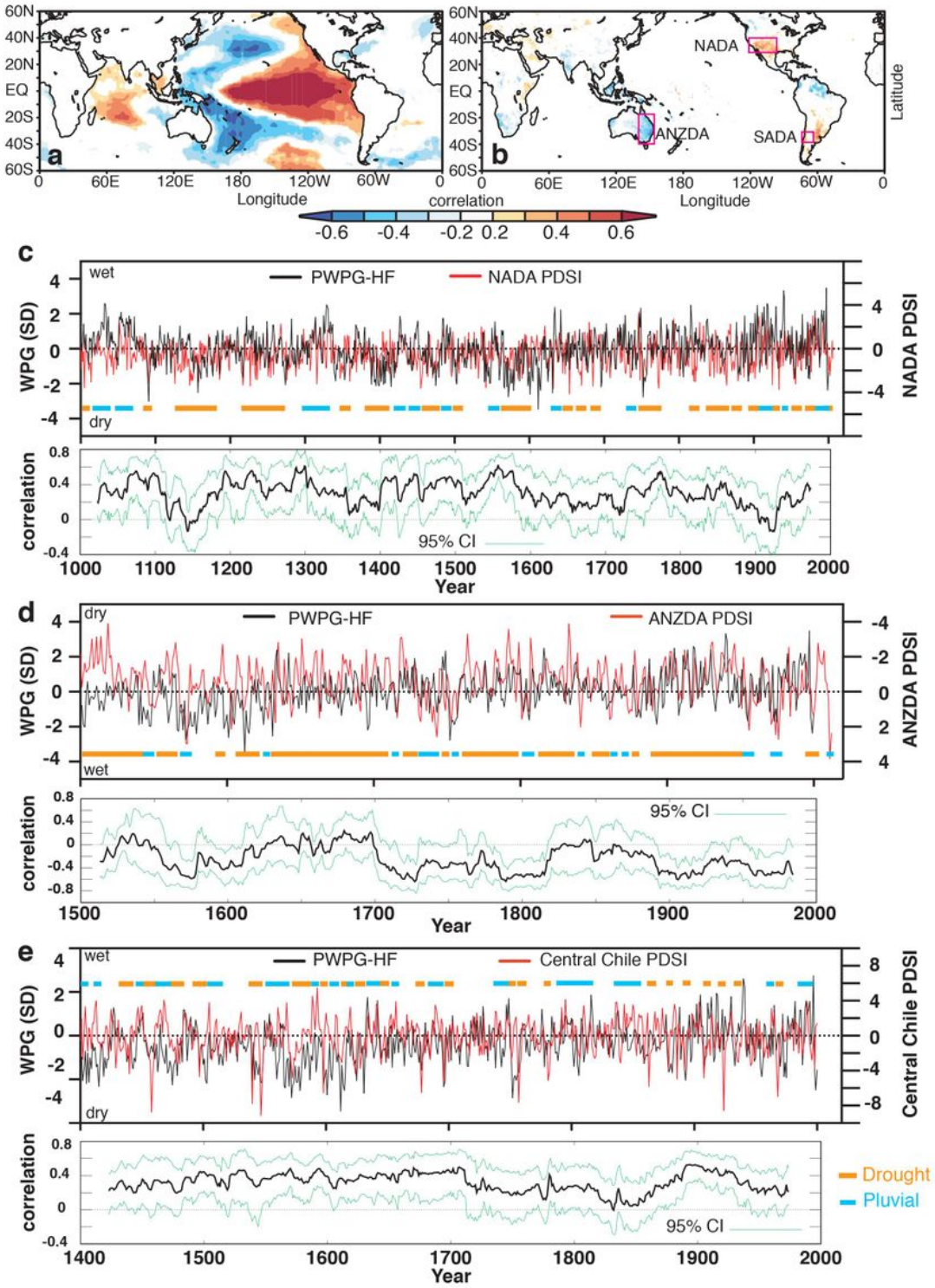

Figure 5

Comparison between the West Pacific Gradient (WPG) reconstruction from PHYDA and palaeohydrological data. a) Spatial correlations between the PHYDA-West Pacific Gradient (PWPG-HF) reconstruction (after Hoell & Funk, 2013) with instrumental HadISST and b) with GPCC rainfall (Schneider

et al., 2010). Only correlation >95% significance coloured. Correlations computed in knmi climate explorer (Trouet & Oldenborgh, 2013). PHYDA-WPG (PWPG-HF) compared to c) North American drought atlas (30-40°N, 125-105°W; Cook et al., 2010) and 51-year running correlation, d) Australia-Nea Zealand drought atlas PDSI (18-29°S, 140-155°E; ANZDA) and 51-year running correlation, and e) Central Chile PDSI from the South America Drought Atlas (31-37°S, 70-72°W; SADA) and 51-year running correlation. Droughts (orange) and pluvials (blue) are indicated.

Supplementary Files

This is a list of supplementary files associated with this preprint. Click to download.

- ZinkeetalSupplementaryFigures.pdf